Published in final edited form as:
J Am Chem Soc. 2009 June 17; 131(23): 8252–8261. doi:10.1021/ja9010095.

Three-Dimensional Structure and Orientation of Rat Islet Amyloid Polypeptide Protein in a Membrane Environment by Solution NMR Spectroscopy

Ravi Prakash Reddy Nanga[†], **Jeffrey R. Brender**[†], **Jiadi Xu**[†], **Kevin Hartman**[†], **Vivekanandan Subramanian**[‡], and **Ayyalusamy Ramamoorthy**[*,†]
Department of Chemistry and Biophysics, University of Michigan, Ann Arbor, Michigan 48109, and Structural Biology/NMR Spectroscopy, U.S. Food and Drug Administration, Bethesda, Maryland 20892

Abstract

Islet amyloid polypeptide (IAPP or amylin) is a 37-residue peptide hormone associated with glucose metabolism that is cosecreted with insulin by β-cells in the pancreas. Since human IAPP is a highly amyloidogenic peptide, it has been suggested that the formation of IAPP amyloid fibers is responsible for the death of β-cells during the early stages of type II diabetes. It has been hypothesized that transient membrane-bound α-helical structures of human IAPP are precursors to the formation of these amyloid deposits. On the other hand, rat IAPP forms transient α-helical structures but does not progress further to form amyloid fibrils. To understand the nature of this intermediate state and the difference in toxicity between the rat and human versions of IAPP, we have solved the high-resolution structure of rat IAPP in the membrane-mimicking detergent micelles composed of dodecylphosphocholine. The structure is characterized by a helical region spanning the residues A5 to S23 and a disordered C-terminus. A distortion in the helix is seen at R18 and S19 that may be involved in receptor binding. Paramagnetic quenching NMR experiments indicate that rat IAPP is bound on the surface of the micelle, in agreement with other nontoxic forms of IAPP. A comparison to the detergent-bound structures of other IAPP variants indicates that the N-terminal region may play a crucial role in the self-association and toxicity of IAPP by controlling access to the putative dimerization interface on the hydrophobic face of the amphipathic helix.

Introduction

Islet amyloid polypeptide (IAPP; also known as amylin) is the major component of amyloid deposits found in the pancreas of type II diabetic patients. Since amyloid deposits are observed in approximately 95% of diabetic patients but are rarely found in nondiabetic individuals, it has been hypothesized that IAPP fibrillization is involved in the pathogenic development of the disease.4–6 More specifically, aggregates of IAPP have been implicated in the loss of β-cell mass and a reduction in insulin production.1 Disruption of the β-cell

ramamoor@umich.edu.
[†]University of Michigan.
[‡]U.S. Food and Drug Administration.

membrane is central to this process.2,3 IAPP oligomers, but not the mature amyloid fibers, have been shown to induce apoptosis by the disruption of calcium homeostasis and the creation of oxidative stress. The mechanism of membrane disruption by IAPP and other amyloid proteins is still a subject of considerable debate.4,5,3

A cross-species comparison of IAPP sequences has shown an interesting correlation between the occurrence of a type II-like form of diabetes and the propensity of the corresponding IAPP sequence to form amyloid fibers. Humans, nonhuman primates, and cats all have amyloidogenic forms of IAPP. Revealingly, a type II diabetic-like syndrome has been observed in all these mammals. Out of the nonamyloidogenic forms of IAPP, the rat variant (rIAPP, sequence shown in Figure 1) has been the most intensively studied. In contrast to the human form of IAPP (hIAPP), rIAPP is almost completely nontoxic to β-cells even at high concentrations. Significantly, rats do not develop diabetes-like symptoms even when rIAPP is overexpressed.6

The nontoxicity of rIAPP has usually been attributed to its inability to form the β-sheet amyloid fibers characteristic of hIAPP. However, mature amyloid fibers are relatively inert compared to the high toxicity exhibited by prefibrillar oligomeric species. Protofibrillar intermediates have been implicated in disturbing cellular homeostasis by disrupting the cellular membrane, either through the formation of ion channels or by a nonspecific general disruption of the lipid bilayer. The structure of the earlier intermediate species is unknown. The sequence of rIAPP differs from hIAPP primarily by the substitution of prolines for critical residues in the amyloidogenic region of hIAPP.7,8 Since prolines act as β-sheet breakers, the absence of rIAPP cytotoxicity has been interpreted as evidence for the theory that the highly toxic prefibrillar intermediates of IAPP possess a similar β-sheet-enriched structure as the mature hIAPP fiber. However, membrane disruption by hIAPP is a complex process with contributions from multiple conformations and multiple oligomeric states.3 In particular, an initial increase in the permeability of the membrane occurs immediately upon the addition of the peptide to the membrane.9 This is followed by a larger increase in permeability, corresponding to a complete disruption of the membrane that is correlated with the formation of amyloid fibers.4,10–13 The biphasic nature of membrane disruption is mirrored by biphasic changes in the conformation of the peptide. Both rIAPP and hIAPP are predominantly α-helical when initially bound to the membrane, as shown for rIAPP in this study and by circular dichroism (CD) and electron paramagnetic resonance (EPR) data for hIAPP bound to phospholipid vesicles.9,14–16 From this α-helical intermediate state, both rIAPP and hIAPP then aggregate to form β-sheet fibers. The initial increase in membrane permeability after IAPP binding may be linked to the formation of pores caused by the self-association of several α-helical IAPP monomers on the membrane.9

The importance of these helical intermediate states of IAPP has been shown by fragments of IAPP ($IAPP_{1-19}$) which form the helical intermediate state when bound to the membrane but do not progress from this state to form amyloid fibers.17–19 The toxicity of these fragments mirrors the relative toxicity of the full-length versions of IAPP.17,19 Rat $IAPP_{1-19}$ is significantly less toxic than $hIAPP_{1-19}$, despite differing from $hIAPP_{1-19}$ by only one residue (a substitution of arginine for histidine at residue 18). Although $rIAPP_{1-19}$ is less toxic to β-cells than $hIAPP_{1-19}$, it is still considerably more toxic than $rIAPP_{1-37}$,

which does not disrupt membranes of less than 50% anionic lipid content (the typical range for a β-cell is 10–20%).20 The amyloidogenic propensity of hIAPP may be seen in this sense as sufficient, but not necessary, for membrane disruption.

To understand how structural differences in the initial helical state may affect the formation of later aggregates and the process of membrane disruption by IAPP, we have solved the high-resolution structure of rIAPP in dodecylphosphocholine (DPC) micelles from two-dimensional (2D) NMR experiments. Previous studies have shown interesting differences between the transient helical conformational states in rIAPP and hIAPP; however, the transient nature of these states has prevented the collection of sufficient distant constraints to create a high-resolution structure.21,22 The high-resolution structure reported here also gives insight into the interaction of IAPP with its membrane-bound G-coupled protein receptor.

Materials and Methods

NMR Sample Preparation

Rat IAPP amidated at the C-terminus was synthesized and purified by GenScript. The purity of the peptide was checked by analytical HPLC. The homogeneity and purity of the peptide sample was also proved by NMR experiments. The formation of the intramolecular disulfide bond from residues 2–7 was verified by electrospray mass spectroscopy. The lyophilized peptide was dissolved in hexafluoroisopropyl alcohol at a concentration of 10 mg/mL and then lyophilized overnight under vacuum to completely remove the solvent. Samples were prepared for NMR measurements by dissolving 3 mg of lyophilized peptide in 20 mM phosphate buffer at pH ~7.3 containing 10% D_2O, 120 mM NaCl, and 200 mM perdeuterated DPC (Cambridge Isotopes Laboratory) to a final concentration of 2.5 mM. IAPP–DPC samples were tested for stability before and after NMR experiments using CD experiments at different temperatures.

NMR Data Collection and Processing

All NMR spectra of IAPP embedded in DPC micelles were recorded at 30 °C using a Bruker spectrometer operating at a ^1H resonance frequency of 900 MHz equipped with a triple-resonance *z*-gradient cryogenic probe optimized for ^1H detection. The 2D TOCSY (total correlation spectroscopy) spectrum of the sample was obtained for a 70 ms mixing time using 512 experiments in the indirect dimension, each with 32 scans and a recycle delay of 2 s. 2D ^1H–^1H NOESY (nuclear Overhauser enhancement spectroscopy) spectra of the same sample were obtained for 100 and 300 ms mixing times using 512 experiments in the indirect dimension, each with 64 scans and a recycle delay of 2 s. Complex data points were acquired for quadrature detection in both the frequency dimensions of these 2D experiments. All spectra were zero-filled in both dimensions to yield matrices of 2048 × 2048 points. Both TOCSY and NOESY spectra were used in the complete assignment of backbone and side-chain resonances. Proton chemical shifts were referenced to the water proton signal at 4.7 ppm (at 30 °C). All 2D spectra were processed using NMRPIPE and TopSpin software from Bruker and analyzed using SPARKY.23,24 Resonance assignment was carried out using a standard approach reported elsewhere.25

Structure Calculations

Structure calculations were performed using the X-PLOR-NIH program. An extended structure of rIAPP was used as a starting point for the hybrid molecular dynamics simulated annealing (SA) protocol at a temperature of 4000 K for the generation of an initial 100 structures.26,27 Subsequently, these structures were refined using a further SA step and energy minimization. The final refinement was carried out using the refine_gentle.inp protocol, which gradually introduces the van der Waals radii. A total of 485 NOEs from the rat IAPP were classified into three distance categories according to their peak intensities obtained from SPARKY analysis–strong (1.8–2.9 Å), medium (1.8–4.5 Å), and weak (1.8–6.0 Å)–and used in the structure calculations of which 262 were intraresidue and 223 inter-residue NOEs (Table 1). The torsion angle restraints were obtained from the TALOS module (http://spin.niddk.nih.gov/bax/software/TALOS) in NMRPIPE using the H^{α} chemical shift values.28 The few ambiguous angles found in the loop region were assigned an additional 60° of conformational freedom compared to their predicted values. Of the 100 structures generated, the 10 lowest energy structures were selected for further analysis. Those structures selected had no violations of (a) NOE constraints higher than 0.5 Å, (b) bond angles higher than 5°, and (c) bond lengths higher than 0.05 Å. The covalent geometry of the conformers generated was determined using PROCHECK_NMR.29

Paramagnetic Quenching

One-dimensional ^{1}H chemical shift spectra of rat IAPP in DPC micelles at concentrations of 0.4, 0.8, and 1.2 mM $MnCl_2$ and at a pH of 7.3 were obtained. All other experimental conditions were the same as mentioned above.

Differential Scanning Calorimetry

Multilamellar vesicle samples for differential scanning calorimetry (DSC) experiments were prepared by first mixing rIAPP in methanol with DMPC/DMPG (7:3) in chloroform. Samples were then vortexed and dried under a stream of nitrogen gas to create a lipid–peptide film. Residual solvent was removed from the film by placing the samples under high vacuum overnight. After the drying process, sodium phosphate buffer (50 mM Na_2PO_4 with 150 mM NaCl at pH 7.3) was added to the dry lipid film, followed by vortexing, several freeze–thaw cycles, and brief sonication. The total molar concentration of lipid was kept constant (5.9 mM) for each sample while the molar peptide concentration was varied as indicated. A total of four heating and four cooling scans were run with a temperature range of 5–45 °C. The heating scans were run at 0.25 °C/min, whereas the cooling scans were run at 1.0 °C/min with a 10 min equilibration period between scans. The data was converted to molar heat capacity using the average molecular weight of the lipids, the lipid concentration, and a partial specific volume of 0.988 mL/g for the lipid mixture. Excess heat capacity was calculated by subtracting a baseline with buffer in both the reference and sample cells at the same scanning rate.

Results

Assignments and Constraints

Micelles containing the detergent DPC and the rat IAPP were prepared for NMR measurements as mentioned in the previous section. As with all membrane-bound peptides, sample preparation is a key step in obtaining the high-resolution spectra of rat IAPP. In our analysis of different experimental conditions, we determined that rat IAPP behaves well with DPC, giving rise to very well-resolved and unique resonances for each of the amide sites in the 2D TOCSY spectrum. In an effort to optimize spectral resolution and sensitivity, several 1D ^{1}H spectra were acquired over a temperature range of 25–45 °C. Only marginal chemical shift changes were observed for the N- and C-termini and the more solvent-exposed residues (residues 24–37), whereas the majority of the residues did not exhibit any chemical shift variation. This demonstrates that the structure is essentially the same at all the temperatures analyzed. The best compromise between resolution and sensitivity was found to be at 30 °C, and we have chosen this temperature to carry out our NMR experiments. Since IAPP peptides are known to aggregate, the micelles were further tested for stability using CD experiments at different temperatures (data not shown). The CD spectra suggested that the rIAPP–DPC micelle was quite stable even after several months and the peptide had significant helical structure in micelles, indicating that rIAPP remained bound to the DPC micelle. Therefore, it was concluded that the sample was suitable for NMR measurements to determine the high-resolution structure and topology of the membrane-associated peptide.

A combination of 2D ^{1}H–^{1}H TOCSY and 2D ^{1}H–^{1}H NOESY spectra was used for the assignment of backbone and side-chain resonances. The 2D ^{1}H–^{1}H NOESY spectra of the rat IAPP obtained in deuterated DPC micelles at pH 7.3 displays numerous, well-resolved cross-peaks, with more than 1.00 ppm spectral dispersion in the amide region indicating that the peptide is well-folded. This spectrum demonstrates numerous NOEs such as $d_{NN}(i, i + 1)$ and $d_{\alpha N}(i, i + 3)$ that are diagnostic for α-helices as shown in Figure 2. The sequential assignments were accomplished using the amide proton to α-proton region of the 2D ^{1}H–^{1}H NOESY spectrum obtained at a 300 ms mixing time. Spectra obtained at mixing times of 100 and 300 ms were nearly identical, except that the longer mixing time produced relatively stronger cross-peaks. The α-proton chemical shift index (CSI) plot for the rat IAPP is given in Figure 3. Chemical shift values for α-protons were not observed for residues K1, C2, and P28, most likely due to fast relaxation suppressing the signal intensity for these residues. Due to high quality of the spectra, the assignment of resonances was straightforward, with the exception of residues in the flexible C-terminal region of the peptide. The fingerprint region of the assigned 2D NOESY spectrum of the peptide obtained at a 300 ms mixing time is shown in Figure 4. We have identified and assigned a total of 485 (262 intraresidue and 223 inter-residue) NOEs from the analysis of the 2D ^{1}H–^{1}H NOESY spectrum. A summary of backbone NOEs for the secondary structure assignment with a histogram indicating the number of NOEs per residue is given in Figure 5. From the density of $d_{\alpha N}(i, i + 1)$, $d_{NN}(i, i + 1)$, and $d_{\beta N}(i, i + 1)$ NOE correlations, it is possible to identify three distinct regions: an N-terminal helix encompassing Ala5–Val17, a short helix from Ser20–Leu23, and a third, long flexible loop region consisting of residues 24–37. Taken together, the NOE and CSI data support the presence of a predominantly α-helical structure

within the Ala5–Leu23 region, with the stretch of residues from Ala5–Val17 and Ser20–Leu23 acting as a more stable core. The remainder of the peptide on the C-terminal end from Gly24–Tyr37 is predominantly disordered. The rmsd analysis supports the presence of higher disorder at the C-terminus of the helical region. The rmsd between structures is 0.52 ± 0.19 for the C_α backbone atoms and 1.24 ± 0.21 for all heavy atoms from residues 5–23. For the C_α atoms of N-terminal well-ordered region (residues 5–17), the calculated rmsd decreases to 0.22 ± 0.07 and 0.72 ± 0.15 for the backbone and heavy atoms, respectively. This difference in backbone rmsd clearly shows that the 5–17 region of rat IAPP is relatively stable and that the helical region from residues 18–23 is more disordered. The overlays of the backbone and side-chain heavy atoms for the final selected conformers are shown in Figure 6. The secondary structure representation of rIAPP is shown in Figure 6C.

All the measured distances and predicted dihedral angles were subsequently modeled using SA calculations with the XPLOR-NIH program. The Ramachandran plots generated using PROCHECK_NMR of the 10 lowest energy structures show that residues V26, L27, T30, and S34 fall in the disallowed region of the Ramachandran plot. This is most likely due to the high mobility of the C-terminal region as well as the presence of the proline residues (P25, P28, and P29) toward the C-terminal end of the peptide.

Positioning of rIAPP in the Micelle

A first approximation of the membrane orientation of rIAPP was obtained using the paramagnetic quencher Mn^{2+} to identify those residues of the peptide that are exposed to solvent. Paramagnetic manganese ions decrease the signal intensity of nuclei that are in close proximity to the ion by increasing the relaxation rate. Because manganese ions cannot penetrate into the hydrophobic interior of the micelle, changes in signal intensity reflect the exposure of the amino acid residues of the peptide to the solvent. The 1D ^1H chemical shift spectra of DPC micelles containing rIAPP and varying concentrations of $MnCl_2$ (0.4, 0.8, and 1.2 mM) are given in Figure 7. The considerable shift and broadening of peaks from micelles containing rat IAPP at low concentrations of $MnCl_2$ suggest that the peptide is in general well-exposed to the water phase and not deeply buried in the hydrophobic core of the micelle. To identify the exposure of specific residues to solvent more precisely, 2D ^1H–^1H TOCSY spectra were used to monitor the changes in the chemical shift and signal intensity of individual α-proton peaks after the addition of 0.8 mm $MnCl_2$. The percentage decrease in the signal intensity of the α-proton chemical shift resonances calculated from the TOCSY spectra is given in Figure 8. Exact intensity calculations could not be made for some residues, either due to overlapping chemical shifts (A13 with G33 and F15 with L23) or the absence of peaks in the ^1H–^1H TOCSY spectrum even without paramagnetic ions (K1, C2, R11, N22, G24, P25, P28, P29, and N35), and therefore the quenching data for these residues is not included in the plot. It is interesting to note that the decrease in the intensity of the α-proton chemical shift resonances upon the addition of the quencher is less in the stable helix located toward the N-terminal region (A5–V17) than in the flexible but structured helix (R18–L23) and the unstructured C-terminus (G24–Y37), indicating that the C-terminal region is significantly more exposed to the solvent. Thus, the site-specific paramagnetic quenching results clearly indicate that the N-terminal part of rat IAPP is a stable helix that is bound to the surface of the membrane, whereas the C-terminal

is mobile and is exposed to the solvent, as supported by the random coil structure as well as the large decrease in signal intensity of α-proton chemical shift resonances upon exposure to paramagnetic quencher $MnCl_2$.

Differential Scanning Calorimetry of rIAPP in Vesicles

The interaction of rIAPP with phospholipid membranes was also characterized by alterations of the main phase transition as detected by differential scanning calorimetry. The main phase transition is associated with the melting of the acyl chains in the hydrophobic core of the membrane from the rigid gel phase to the more fluid liquid-crystalline phase. This phase transition is sensitive to the binding of peptides to the membrane, in particular to the depth at which the peptide penetrates into the bilayer. The degree of perturbation of the phase transition is correlated with the displacement of the acyl chains of the lipid and is strongest if the peptide localizes in the bilayer at the glycerol region preceding the acyl chains and less for peptides that bind only at the top of the bilayer or insert into the membrane in a transmembrane orientation.30–32 Rat IAPP reduces the phase transition temperature (melting temperature (Tm), enthalpy change (ΔH, equal to the area of the transition on the thermogram), and cooperativity of the transition (related to the width of the transition) (Figure 9). The transition is asymmetric at higher concentrations (>1.0% rIAPP), suggesting rIAPP may be forming peptide-rich domains or forming clusters of DMPG-rich domains.19 The degree of reduction is significant, but less than that observed for peptides known to bind near the glycerol region.33–35 Taken together with the paramagnetic quenching data, DSC suggests rIAPP binds at the surface of the membrane with the disordered loop extending into the solvent.

Discussion

Early intermediates in the misfolding pathway have been implicated in pathogenesis of a growing number of common and devastating diseases such as type II diabetes, Alzheimer's disease, and Parkinson's disease. Since damage to the cellular membrane has been identified as a major source of the toxicity of amyloid proteins, it has been recognized that solving the atomic-level resolution structures of amyloid peptides and proteins in a membrane environment would provide insights into their toxic properties.36–41 Such atomic-level resolution structural insights will enable the design of compounds to suppress the toxicity of amyloids and will therefore aid the design of drugs to treat amyloid diseases. Unfortunately, structural studies have been difficult as these systems are not amenable for X-ray diffraction studies due to the difficulty in obtaining high-quality single crystals. In this study, we have investigated the 3D structure of rIAPP in a detergent micelle using NMR spectroscopy in order to understand the folding of intermediates of IAPP in membrane and the origin of toxicity of the hIAPP peptide by looking at its nontoxic rIAPP counterpart which forms similar folding intermediates and can disrupt membranes under certain conditions.9,11,15

The high-resolution structure of membrane-bound rIAPP determined here resembles the transient helical forms of both rIAPP and hIAPP in solution, with some differences as outlined below.21,22 The structure of rIAPP in DPC micelles is dominated by a N-terminal helical region from residues A5 to S23 and a disordered C-terminus. In solution, the helical

region of rIAPP is shorter than in the membrane-bound form, spanning residues 5–19, whereas residues 20–23 are involved in hydrogen-bonding interactions with the helix but do not adopt a helical conformation.22 Human IAPP, which lacks the conformational restraints imposed by the three prolines in rIAPP, has a greater helical propensity in solution that extends throughout the entire molecule except for the N-terminal ring which is conformationally constrained by the disulfide bond between residues 2 and 7.21 The helical propensity for hIAPP in solution is greatest, however, in the N-terminal section up to residue 20 which is similar to the results presented here.21

Some hypotheses about the driving force for membrane-catalyzed aggregation can be directly supported by comparing the rIAPP with the very recently solved structure of unamidated hIAPP in SDS micelles.42 The structure of hIAPP bound to SDS has an overall fold similar to that of rIAPP in DPC micelles, consisting of an ordered N-terminal helix, a flexible hinge region, and a less ordered helix that is followed by a disordered C-terminus. The N-terminal helical region in the rIAPP structure (5–17) corresponds to a similar stretch of helical residues in the hIAPP structure (5–17) as well as in a lower resolution EPR study of spin-labeled hIAPP bound to small unilamellar vesicles (9–22), as can be expected by the very high degree of sequence homology in this region.14 A flexible region that corresponds to the center of the loop in the β-hairpin structure of the IAPP amyloid fiber is seen in both structures.43–45 This hinge may also have implications for the binding of IAPP to its receptor as discussed below. The major difference between the two structures is in the C-terminal region, which is completely disordered in the rIAPP structure but consists of a dynamic helix (S20–L27) followed by a disordered C-terminal tail in the hIAPP structure. Membrane-catalyzed aggregation is believed to proceed first by the association of the helical regions of the peptide, followed by the formation of β-sheet structure in the disordered regions.9,46 The formation of secondary structure in unstructured regions of the peptide upon self-association is believed to be a major contributor to the binding energy of hIAPP to membranes and is also thought to be responsible for the cooperativity seen in the binding of hIAPP to membranes.9 Our structure confirms that a large section of the rIAPP peptide remains unstructured when bound to the membrane. The lesser degree of structure in the C-terminus of rIAPP is likely to impact the early self-association of rIAPP in several ways. First, it is probable that the additional helix present in the hIAPP structure provides an additional ordered interaction surface to nucleate self-association. Second, if the C-terminus of rIAPP cannot form ordered structures, as the DPC micelle bound peptide structure indicates, a large contribution to energy of self-association is lost. It has been shown that proline mutations outside the amyloidogenic region of IAPP (proline substitutions at positions 17, 19, and 30) result in a large inhibition of amyloid formation and the loss of amyloid fiber stability.47 In light of the differences between rIAPP and hIAPP structures in the C-terminal region, it would be interesting to further investigate the effect of mutations that stabilize or destabilize secondary structure specifically in this region.48,49

In solution, the prolines of rIAPP are predominantly, but not exclusively, in the trans conformation. A small percentage of the P25 and P28 residues, but not P29, are in the cis conformation as shown by the observation of α–α NOE connectivities for P25 and P28 that are diagnostic for the cis conformation.22 The prolines in the membrane-bound form have a

stronger preference for the trans conformation than those in rIAPP in solution as multiple resonances are only seen for V26, and not for G24 and L27. This indicates P28 and P29 are exclusively in the trans conformation when bound to the membrane, and only P25 is undergoing slow cis/trans isomerization. The C-terminal residues of rIAPP from T30 are in an extended, disordered conformation extending outward from the helix. The disordered C-terminus does not interact with any other part of the rIAPP molecule, as shown by the absence of long- or medium-range NOEs. Rat IAPP is a monomer in the micelle as shown by the absence of long-range NOEs for the side-chain atoms.

Rat IAPP Binds to the Surface of the Micelle in an Orientation That Has Been Associated with Low Cytotoxicity in Other Amyloid Peptides

Most of the residues in rIAPP are highly quenched by the water-soluble Mn^{2+} ion. Since the Mn^{2+} ion cannot penetrate into the hydrophobic core of the micelle, this result indicates most of the residues in rIAPP are located at solvent-accessible sites in the micelle. A peptide bound to the surface of the micelle will have a periodic quenching efficiency reflective of the asymmetric solvent exposure of the two faces of the helix. On the other hand, a helix that is deeply inserted into the micelle will be largely insensitive to the presence of Mn^{2+} ions, except for residues at the ends of the helix that extend into the solvent or into the interfacial region of the micelle. In the rIAPP sample, the quenching efficiency oscillates periodically in the main helical region from T6 to approximately R18, with maximal quenching occurring approximately every $i + 4$ residues as is expected for a surface-bound α-helix (Figure 8). The existence of highly quenched residues also indicates rIAPP is relatively tightly bound to the micelle and not dissociating from the surface despite the neutral overall charge on DPC. The unstructured C-terminus (G24–Y37) of the peptide is almost completely quenched by Mn^{2+}, indicating this region extends out of the micelle into the solvent (Figure 10). Although the orientation of the N-terminal region cannot be directly determined from the quenching data due to the lack of signal in this area, it can be inferred that this region curves toward the micelle based on the hydrophobicity of these residues.

The importance of membrane binding topology in controlling the toxicity of IAPP has been illustrated by experiments on the rat and human versions of the $IAPP_{1-19}$ fragment. Human IAPP and $hIAPP_{1-19}$ have similar toxicity to β-cells.17 The analogous $rIAPP_{1-19}$ peptide is significantly less toxic despite differing from $hIAPP_{1-19}$ only by the single substitution of Arg for His at residue 18 and can only disrupt membranes at high peptide-to-lipid ratios which are likely to facilitate peptide oligomerization and membrane insertion.19 This difference in toxicity of the two peptides is associated with a corresponding difference in membrane binding topologies. At neutral pH, $hIAPP_{1-19}$ is buried within the micelle, whereas $rIAPP_{1-19}$ adopts a surface-associated binding mode. Protonation of H18 in $hIAPP_{1-19}$ moves the peptide to the surface of the micelle and is accompanied by a corresponding decrease in toxicity.18,19 Neutron diffraction, fluorescence anisotropy measurements, and analysis of packing density all suggest a similar, deeply inserted binding mode for the full-length human IAPP peptide.9,16,50 Although EPR quenching experiments have shown a surface-associated topology for hIAPP at low peptide-to-lipid ratios,14 it is likely that this topology is associated with peptide in a monomeric form that is associated with low toxicity.9,19

Differences in the Position and Flexibility of the N-Terminal Loop Contribute to Differences in Self-Association for IAPP Variants

The differences in the location of the peptides within the membrane observed are insufficient to explain the relative toxicity of IAPP variants. Although both rIAPP$_{1-19}$ and full-length rIAPP adopt a surface-associated orientation, there are still significant differences in toxicity between the two peptides.19 Although the full-length rIAPP peptide is almost entirely nontoxic, rIAPP$_{1-19}$ is moderately toxic to β-cells. Significantly, rIAPP$_{1-19}$ can disrupt membranes at high peptide-to-lipid ratios, suggesting that although membrane-mediated oligomerization is impaired in rIAPP$_{1-19}$ it is not almost entirely absent as it is in rIAPP. Membrane insertion cannot easily occur for IAPP without oligomerization, as the charged arginine (R11) in the middle of the amphipathic helix cannot be buried in the membrane without the formation of a water-filled channel or major distortions of the bilayer. As oligomerization is essential for cooperative membrane binding and membrane disruption, structural differences in rIAPP which affect self-association may explain the lack of toxicity of this peptide. Aggregation of the IAPP peptide is believed to be mediated by favorable coiled-coil interactions among the leucine residues located on the hydrophobic face of the amphipathic helix.9 Blockage of this site can therefore be expected to be associated with a decrease in self-association and toxicity. Intriguingly, both properties correlate with the position and flexibility of the N-terminal loop (residues 2–7). In all the membrane-bound IAPP structures solved thus far, this region adopts a loosely coiled conformation due to the structural constraints imposed by the C2–C7 disulfide bridge. In the structure of the highly toxic hIAPP and hIAPP$_{1-19}$ peptides, the N-terminal loop is bent away from the hydrophobic interface.18 In this position the hydrophobic side of the helix is exposed and can mediate hydrophobic interactions that favor the formation of a helical bundle (Figure 11, parts A and B, respectively). Conversely, in the structure of nontoxic rIAPP this loop is bent toward the hydrophobic face of the helix in a manner that would block binding of IAPP to the hydrophobic face of the helix (see Figure 11C). The N-terminus of moderately toxic rIAPP$_{1-19}$ is also tilted toward the hydrophobic face of the helical region (Figure 11D).18 However, the N-terminal loop of rIAPP$_{1-19}$ is considerably more flexible than that of rIAPP. The extra flexibility in the N-terminus of rIAPP$_{1-19}$ is likely to facilitate a movement of this region away from the hydrophobic face of the helix upon dimerization. The greater rigidity of the rIAPP N-terminal loop can be seen by a comparison of the NOEs in this region. The N-terminal loops of both 1–19 fragments are only constrained in by HA–NH connectivity in the residues adjoining the disulfide bridge and not by any constraints within the N-terminal loop itself, indicating a significant degree of flexibility within the N-terminal loop. The full-length rIAPP structure, on the other hand, has several NOEs within the disulfide bridge, indicating a considerably more rigid N-terminus.

The sequences of all the IAPP variants discussed above are identical up to residue 18, and it may seem paradoxical that the N-terminal regions are different in the absence of any tertiary structure in the peptides. The likely source of this difference is alterations in the peptide–membrane interactions, which also aids in explaining the differing propensities of the peptides to aggregate. In solution, rIAPP is prevented from aggregating largely by the conformational restraints imposed by the three proline residues.7,8 However, it is important

to note that hIAPP with triple proline substitutions displays greatly reduced, but still detectable, aggregation.47 This suggests that the charge on R18 and alterations in the N-terminus play some role in the relative aggregation propensity. Aggregation rates are greatly enhanced once the peptide is bound to the membrane due to the concentrating effect of restricting diffusion to a two-dimensional surface and the restriction of angular motion.16,51,52 Several features of the membrane-bound rIAPP act in concert to retard aggregation and the formation of toxic oligomers. First, the charge on R18 inhibits the deep insertion of the peptide into the membrane as seen for the $rIAPP_{1-19}$ peptide.18,19 Furthermore, the disordered C-terminus in rIAPP that is absent in $rIAPP_{1-19}$ compounds the difficulty of membrane insertion as hydrogen bonding of the peptide to solvent cannot be accommodated in the hydrophobic interior of an intact membrane. This difference in the C-terminal end of the peptide likely has the effect of altering the interaction of rIAPP with the membrane compared to $rIAPP_{1-19}$. The likely result of this difference in the interactions of rIAPP, $rIAPP_{1-19}$, $hIAPP_{1-19}$, and most likely hIAPP with the membrane are alterations of the structure and dynamics at the N-terminus, which could impact the self-association of IAPP as discussed above.

Significance of the Structure for the Normal Biological Activity of IAPP

IAPP belongs to the CGRP family of peptides that includes calcitonin-gene-related peptide (CGRP), calcitonin, adrenomodulin, and IAPP.53 Although the sequences of these peptides are somewhat dissimilar, all the peptides in this family bind to common G-coupled protein receptors and produce similar effects in many tissues.54,55 Many of the peptides in this family such as human CGRP and calcitonin are also amyloidogenic and aggregate to form membrane-disruptive oligomeric structures.56–59 NMR studies on these peptides in detergent micelles have shown that these properties are apparently linked to common structural elements held among the family. All of the peptides in this family possess an amidated C-terminus, an amphipathic helix near the N-terminus, a largely disordered C-terminus, and an N-terminal ring connected by a disulfide bond.60–63 Two binding sites have been proposed for the binding of peptides of this family to the membrane-bound receptor: one near the membrane surface that would be consistent with the orientation found in this study for rIAPP and another requiring a more deeply inserted membrane orientation as found for $hIAPP_{1-19}$ and hypothesized for hIAPP.60,64,65 Relatively little is known about structure–activity relationships for IAPP's normal biological action in comparison to its pathological aggregation. Experiments on truncated versions of calcitonin and CGRP (the closest homologue of IAPP) have shown that the formation of the amphipathic helix is sufficient for receptor binding but activation of the receptor requires the N-terminal ring.66 Removal of the N-terminal ring or reduction of the disulfide bridge results in CGRP binding to its receptor in an inactive conformation. A similar N-truncated rIAPP construct ($rIAPP_{8-37}$) has been shown to act as an antagonist for rIAPP's effects on insulin secretion and carbohydrate and lipid metabolism.67–69 Given the importance of the N-terminal ring for the biological activity of IAPP, it would be interesting to further study the biological activity of IAPP in light of the structural differences in the N-terminal ring shown here for rIAPP and $IAPP_{1-19}$ and is hypothesized for hIAPP.70

Several structural features that have been shown to be important for other members of this family are absent in the rIAPP structure. A β-turn centered on P34 has been shown to be important for the activity of the related calcitonin60,71,72 and CGRP peptides.62,73,74 Similar β-turns have been shown to be a common feature for the activation of other peptide-activated G-coupled protein receptors.75 This turn is absent in both the rIAPP and hIAPP structures, although the 20–29 fragment of hIAPP adopts a similar distorted type I β-turn that has been implicated in the binding of IAPP to glycolipids.42,76,77 However, since considerable flexibility exists at this site it is possible that IAPP adopts the β-turn conformation in this region seen in its homologues upon binding to the IAPP receptor. A significant degree of mobility has also been detected by EPR at residues 21 and 22 for hIAPP bound to small unilamellar vesicles.14 An interaction of the disordered C-terminus with the N-terminus has been invoked as contributing to the higher potency of salmon calcitonin over human calcitonin.60,61 This interaction is also absent in rIAPP. The C-terminus of rIAPP is folded away from the helix as in the human calcitonin structure, as indicated by the absence of medium- or long-range NOEs in this region.60

Conclusion

We have solved the first structure of rat IAPP in a membrane environment. By comparing the rIAPP structure with other toxic and nontoxic variants of IAPP, we have identified two structural features that correlate with the toxicity of the peptide. Rat IAPP is bound to the surface in a manner similar to the nontoxic $rIAPP_{1-19}$ and low-pH $hIAPP_{1-19}$ peptides and does not penetrate deeply into the micelle like the toxic neutral pH $hIAPP_{1-19}$ peptide. The position of the N-terminal disulfide bridge has been identified as another factor that may modulate aggregation and toxicity. The nontoxic rIAPP structure has a relatively rigid N-terminus that is bent toward the hydrophobic face of the amphipathic helix, whereas more toxic forms of IAPP have a more flexible N-terminus that is positioned away from the amphipathic helix. A comparison of the rIAPP structure to other homologous peptides that share the same receptors, hIAPP, and also fragments from hIAPP shows rIAPP does not possess the β-turn seen in these peptides that is required to activate the receptor, but this region is flexible and may form a β-turn upon binding to the receptor. Further structural studies on IAPP, in particular with respect to its normal biological activity, will be particularly useful in understanding the effects of this peptide.

Acknowledgments

This study was supported by research funds from NIH (DK078885 to A.R.) and Michigan Diabetes Research Training Center at the University of Michigan.

References

1. Haataja L, Gurlo T, Huang CJ, Butler PC. Endocr Rev. 2008; 29:302–316.
2. Jayasinghe SA, Langen R. Biochim Biophys Acta. 2007; 1768:2002–2009. [PubMed: 17349968]
3. Khemtemourian L, Killian JA, Hoppener JW, Engel MF. Exp Diabetes Res. 2008; 2008:421287. [PubMed: 18483616]
4. Engel MF, Khemtemourian L, Kleijer CC, Meeldijk HJ, Jacobs J, Verkleij AJ, de Kruijff B, Killian JA, Hoppener JW. Proc Natl Acad Sci USA. 2008; 105:6033–6038. [PubMed: 18408164]

5. Quist A, Doudevski L, Lin H, Azimova R, Ng D, Frangione B, Kagan B, Ghiso J, Lal R. Proc Natl Acad Sci USA. 2005; 102:10427–10432. [PubMed: 16020533]
6. Huang CJ, Haataja L, Gurlo T, Butler AE, Wu XJ, Soeller WC, Butlerv PC. Am J Physiol. 2007; 293:E1656–E1662.
7. Westermark P, Engstrom U, Johnson KH, Westermark GT, Betsholtz C. Proc Natl Acad Sci USA. 1990; 87:5036–5040. [PubMed: 2195544]
8. Moriarty DF, Raleigh DP. Biochemistry. 1999; 38:1811–1818. [PubMed: 10026261]
9. Knight JD, Hebda JA, Miranker AD. Biochemistry. 2006; 45:9496–9508. [PubMed: 16878984]
10. Brender JR, Durr UHN, Heyl D, Budarapu MB, Ramamoorthy A. Biochim Biophys Acta. 2007; 1768:2026–2029. [PubMed: 17662957]
11. Green JD, Kreplak L, Goldsbury C, Blatter XL, Stolz M, Cooper GS, Seelig A, Kist-Ler J, Aebi U. J Mol Biol. 2004; 342:877–887. [PubMed: 15342243]
12. Sparr E, Engel MFM, Sakharov DV, Sprong M, Jacobs J, de Kruijff B, Hoppener JWM, Killian JA. FEBS Lett. 2004; 577:117–120. [PubMed: 15527771]
13. Domanov YA, Kinnunen PKJ. J Mol Biol. 2008; 376:42–54. [PubMed: 18155730]
14. Apostolidou M, Jayasinghe SA, Langen R. J Biol Chem. 2008; 283:17205–17210. [PubMed: 18442979]
15. Jayasinghe SA, Langen R. Biochemistry. 2005; 44:12113–12119. [PubMed: 16142909]
16. Knight JD, Miranker AD. J Mol Biol. 2004; 341:1175–1187. [PubMed: 15321714]
17. Brender JR, Lee EL, Cavitt MA, Gafni A, Steel DG, Ramamoorthy A. J Am Chem Soc. 2008; 130:6424–6429. [PubMed: 18444645]
18. Nanga RPR, Brender JR, Xu J, Veglia G, Ramamoorthy A. Biochemistry. 2008; 47:12689–12697. [PubMed: 18989932]
19. Brender JR, Hartman K, Reid KR, Kennedy RT, Ramamoorthy A. Biochemistry. 2008; 47:12680–12689. [PubMed: 18989933]
20. Rustenbeck I, Matthies A, Lenzen S. Lipids. 1994; 29:685–692. [PubMed: 7861935]
21. Yonemoto IT, Kroon GJ, Dyson HJ, Balch WE, Kelly JW. Biochemistry. 2008; 47:9900–9910. [PubMed: 18710262]
22. Williamson JA, Miranker AD. Protein Sci. 2007; 16:110–117. [PubMed: 17123962]
23. Delaglio F, Grzesiek S, Vuister GW, Zhu G, Pfeifer J, Bax A. J Biomol NMR. 1995; 6:277–293. [PubMed: 8520220]
24. Goddard, TD.; Kneller, DG. SPARKY 3. University of California; San Francisco, CA: 1999.
25. Wuthrich, K. NMR of Proteins and Nucleic Acids. John Wiley and Sons; New York: 1986.
26. Nilges M, Gronenborn AM, Brunger AT, Clore GM. Protein Eng. 1988; 2:27–38. [PubMed: 2855369]
27. Stein EG, Rice LM, Brunger AT. J Magn Reson. 1997; 124:154–164. [PubMed: 9424305]
28. Cornilescu G, Delaglio F, Bax A. J Biomol NMR. 1999; 13:289–302. [PubMed: 10212987]
29. Laskowski RA, Rullman JAC, MacArther MW, Kaptein R, Thornton JM. J Biomol NMR. 1998; 8:477–486. [PubMed: 9008363]
30. Pappalardo G, Milardi D, Magri A, Attanasio F, Impellizzeri G, La Rosa C, Grasso D, Rizzarelli E. Chem–Eur J. 2007; 13:10204–10215. [PubMed: 17902185]
31. Grasso D, Milardi D, La Rosa C, Rizzarelli E. New J Chem. 2001; 25:1543–1548.
32. Sciacca MFM, Pappalardo M, Milardi D, Grasso DM, La Rosa C. Arch Biochem Biophys. 2008; 477:291–298. [PubMed: 18621014]
33. Thennarasu S, Lee DK, Poon A, Kawulka KE, Vederas JC, Ramamoorthy A. Chem Phys Lipids. 2005; 137:38–51. [PubMed: 16095584]
34. Hallock KJ, Lee DK, Omnaas J, Mosberg HI, Ramamoorthy A. Biophys J. 2002; 83:1004–1013. [PubMed: 12124282]
35. Henzler-Wildman KA, Martinez GV, Brown MF, Ramamoorthy A. Biochemistry. 2004; 43:8459–8469. [PubMed: 15222757]
36. Coles M, Bicknell W, Watson AA, Fairlie DP, Craik DJ. Biochemistry. 1998; 37:11064–11077. [PubMed: 9693002]

37. Mandal PK, Pettegrew JW. Neurochem Res. 2004; 29:2267–2272. [PubMed: 15672549]
38. Ulmer TS, Bax A. J Biol Chem. 2005; 280:43179–43187. [PubMed: 16166095]
39. Ulmer TS, Bax A, Cole NB, Nussbaum RL. J Biol Chem. 2005; 280:9595–9603. [PubMed: 15615727]
40. Jarvet J, Danielsson J, Damberg P, Oleszczuk M, Graeslund A. J Biomol NMR. 2007; 39:63–72. [PubMed: 17657567]
41. Shao HY, Jao SC, Ma K, Zagorski MG. J Mol Biol. 1999; 285:755–773. [PubMed: 9878442]
42. Patil SM, Xu S, Sheftic SR, Alexandrescu AT. J Biol Chem. 2009; 284:11982–11991. [PubMed: 19244249]
43. Luca S, Yau WM, Leapman R, Tycko R. Biochemistry. 2007; 46:13505–13522. [PubMed: 17979302]
44. Wiltzius JJW, Sievers SA, Sawaya MR, Cascio D, Popov D, Riekel C, Eisenberg D. Protein Sci. 2008; 17:1467–1474. [PubMed: 18556473]
45. Kajava AV, Aebi U, Steven AC. J Mol Biol. 2005; 348:247–252. [PubMed: 15811365]
46. Abedini A, Raleigh DP. Phys Biol. 2009; 6:15005.
47. Abedini A, Raleigh DP. J Mol Biol. 2006; 355:274–281. [PubMed: 16303136]
48. Koo BW, Hebda JA, Miranker AD. Protein Eng, Des Sel. 2008; 21:147–154. [PubMed: 18299291]
49. Green J, Goldsbury C, Min T, Sunderji S, Frey P, Kistler J, Cooper G, Aebi U. J Mol Biol. 2003; 326:1147–1156. [PubMed: 12589759]
50. Balali-Mood K, Ashley RH, Hauss T, Bradshaw JP. FEBS Lett. 2005; 579:1143–1148. [PubMed: 15710403]
51. Bokvist M, Grobner G. J Am Chem Soc. 2007; 129:14848. [PubMed: 17990885]
52. Aisenbrey C, Borowik T, Bystrom R, Bokvist M, Lindstrom F, Misiak H, Sani MA, Grobner G. Eur Biophys J Biophys Lett. 2008; 37:247–255.
53. Wimalawansa SJ. Crit Rev Neurobiol. 1997; 11:167–239. [PubMed: 9209829]
54. Lutz TA, Tschudy S, Rushing PA, Scharrer E. Peptides. 2000; 21:233–238. [PubMed: 10764950]
55. Christopoulos G, Perry KJ, Morfis M, Tilakaratne N, Gao YY, Fraser NJ, Main MJ, Foord SM, Sexton PM. Mol Pharmacol. 1999; 56:235–242. [PubMed: 10385705]
56. Diociaiuti M, Polzi LZ, Valvo L, Malchiodi-Albedi F, Bombelli C. Biophys J. 2006; 91:2275–2281. [PubMed: 16940475]
57. Fowler SB, Poon S, Muff R, Chiti F, Dobson CM, Zurdo J. Proc Natl Acad Sci USA. 2005; 102:10105–10110. [PubMed: 16006528]
58. Micelli S, Meleleo D, Picciarelli V, Gallucci E. Front Biosci. 2006; 11:2035–2044. [PubMed: 16720289]
59. Stipani V, Gallucci E, Micelli S, Picciarelli V, Benz R. Biophys J. 2001; 81:3332–3338. [PubMed: 11720996]
60. Motta A, Andreotti G, Amodeo P, Strazzullo G, Morelli MAC. Proteins. 1998; 32:314–323. [PubMed: 9715908]
61. Motta A, Pastore A, Goud NA, Morelli MAC. Biochemistry. 1991; 30:10444–10450. [PubMed: 1931969]
62. Carpenter KA, Schmidt R, von Mentzer B, Haglund U, Roberts E, Walpole C. Biochemistry. 2001; 40:8317–8325. [PubMed: 11444978]
63. Oconnell JP, Kelly SM, Raleigh DP, Hubbard JAM, Price NC, Dobson CM, Smith BJ. Biochem J. 1993; 291:205–210. [PubMed: 8385932]
64. Morelli MAC, Pastore A, Motta A. J Biomol NMR. 1992; 2:335–348. [PubMed: 1511235]
65. Nakamuta H, Orlowski RC, Epand RM. Endocrinology. 1990; 127:163–169. [PubMed: 2163309]
66. Kapurniotu A. Curr Med Chem. 2004; 11:2845–2865. [PubMed: 15544479]
67. Hettiarachchi M, Chalkley S, Furler SM, Choong YS, Heller M, Cooper GJS, Kraegen EW. Am J Physiol. 1997; 36:E859–E867. [PubMed: 9374670]
68. Wang MW, Young AA, Rink TJ, Cooper GJS. FEBS Lett. 1991; 291:195–198. [PubMed: 1936264]

69. Ye JM, Lim-Fraser M, Cooney GJ, Cooper GJS, Iglesias MA, Watson DG, Choong B, Kraegen EW. Am J Physiol. 2001; 280:E562–E569.

70. Neumann JM, Couvineau A, Murail S, Lacapere JJ, Jamin N, Laburthe M. Trends Biochem Sci. 2008; 33:314–319. [PubMed: 18555686]

71. Kazantzis A, Waldner M, Taylor JW, Kapurniotu A. Eur J Biochem. 2002; 269:780–791. [PubMed: 11846779]

72. Kapurniotu A, Kayed R, Taylor JW, Voelter W. Eur J Biochem. 1999; 265:606–618. [PubMed: 10504392]

73. Lang M, De Pol S, Baldauf C, Hofmann HJ, Reiser O, Beck-Sickinger AG. J Med Chem. 2006; 49:616–624. [PubMed: 16420047]

74. Wisskirchen FM, Doyle PM, Gough SL, Harris CJ, Marshall I. Br J Pharmacol. 1999; 126:1163–1170. [PubMed: 10205004]

75. Tyndall JDA, Pfeiffer B, Abbenante G, Fairlie DP. Chem Rev. 2005; 105:793–826. [PubMed: 15755077]

76. Levy M, Garmy N, Gazit E, Fantini J. FEBS J. 2006; 273:5724–5735. [PubMed: 17212787]

77. (a) Mascioni A, Porcelli F, Ilangovan U, Ramamoorthy A, Veglia G. Biopolymers. 2003; 69:29–41. [PubMed: 12717720] (b) Ilangovan U, Ramamoorthy A. Biopolymers. 1998; 45:9–20. [PubMed: 9433183]

78. Tieleman DP, van der Spoel D, Berendsen HJC. J Phys Chem B. 2000; 104:6380–6388.

Figure 1.

Amino acid sequences of rat and human IAPP with nonconserved residues shown in red color in the rat IAPP sequence. The peptide is amidated at the C-terminus and has a disulfide bridge from C2 to C7 like the physiologically expressed peptide.

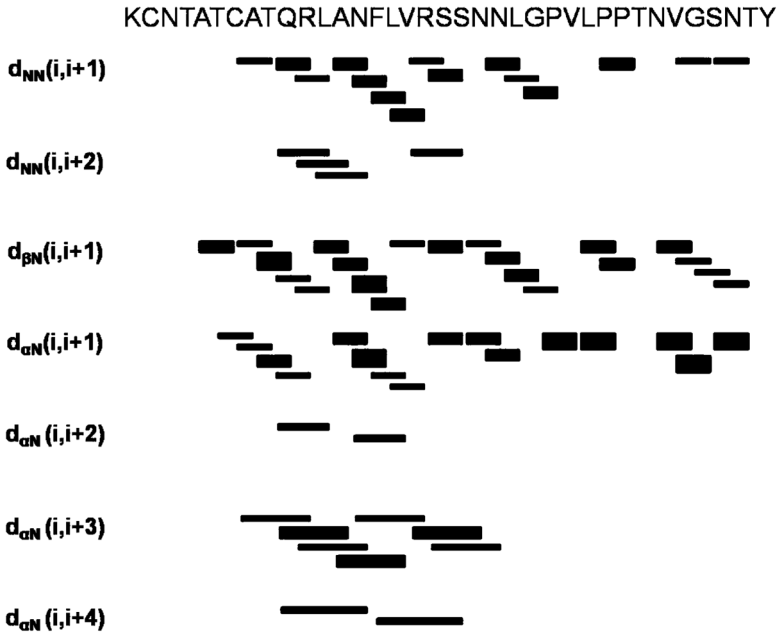

Figure 2.

Summary of the sequential and medium-range NOE connectivities for rIAPP in DPC micelles at 30 °C, pH 7.3. The intensities of the observed NOEs are represented by the thickness of lines and are classified as strong, medium, and weak, corresponding to upper bound constraints of 2.9, 4.5, and 6 Å, respectively.

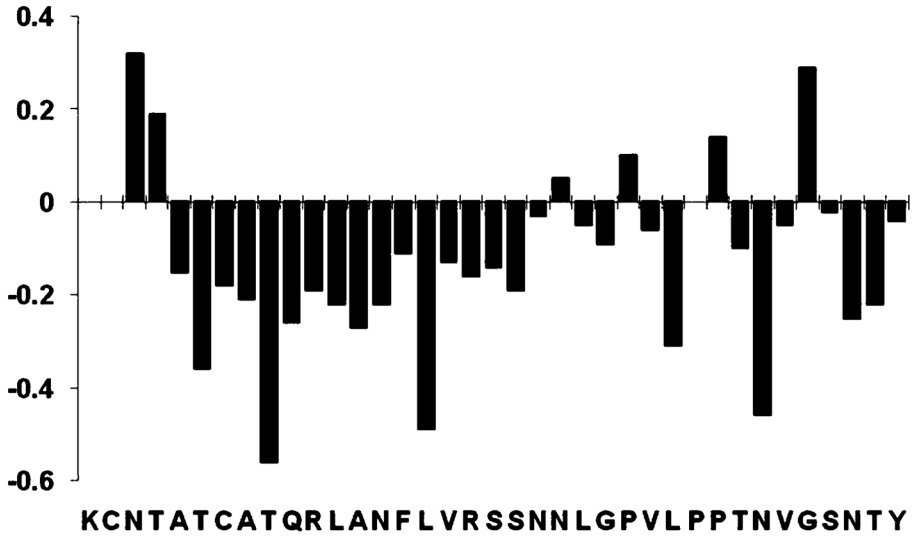

Figure 3.

α-Proton chemical shift index (CSI) for rat IAPP showing the propensity of IAPP to form an α-helix at the N-terminal region of the peptide. The CSI was calculated by subtracting the values measured for the peptide from the random coil shifts reported in the literature (ref 25).

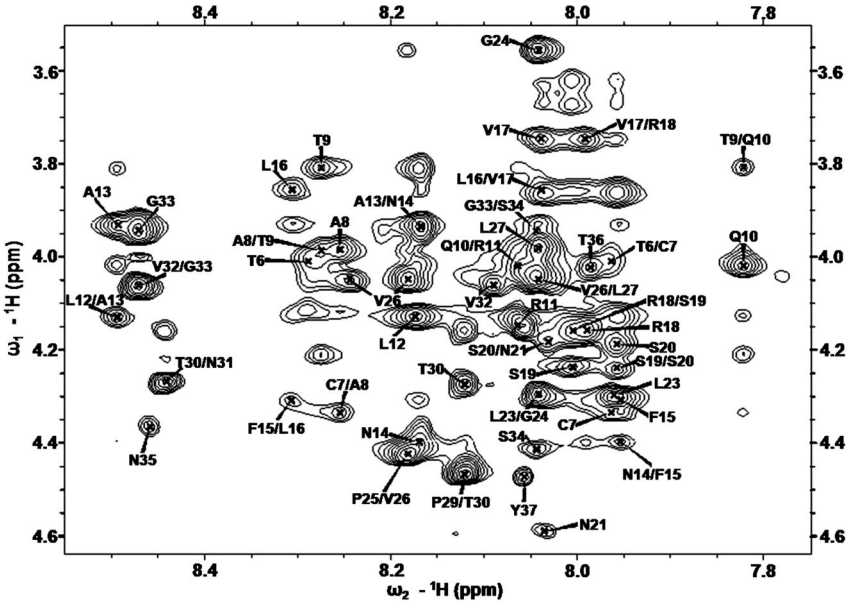

Figure 4.

Fingerprint region of the 2D ^{1}H–^{1}H NOESY spectra of rat IAPP showing the NOE α-proton connectivities. A single resonance was detected for each residue except for Val 26, which has two resonance peaks.

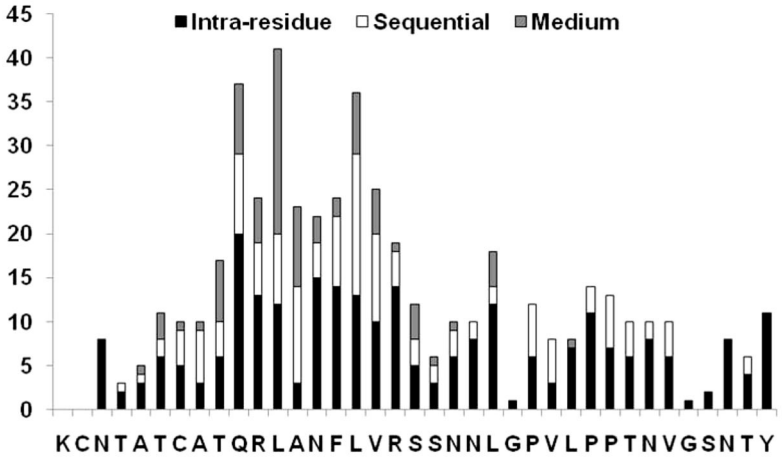

Figure 5.

Histogram of NOEs vs the residue number for rat IAPP, showing the number of intraresidue, sequential ($i - j = 1$), and medium-range ($i - j = 2, 3, 4$) NOEs. Long-range ($i - j > 4$) NOEs were not observed.

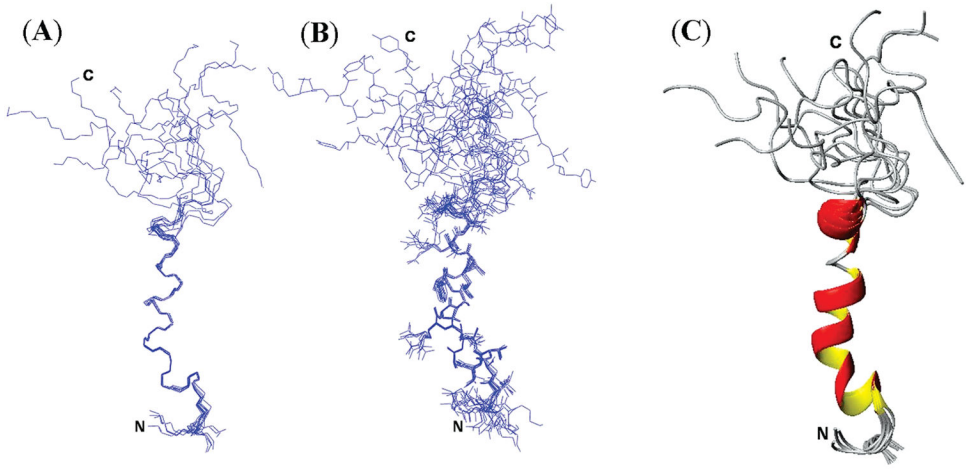

Figure 6.

Ensembles of conformers for rat IAPP showing the convergence of conformers for backbone atoms (A) and side-chain atoms (B). (C) Secondary structure representation of an overlaid ensemble of conformers for rat IAPP. Two helices, an ordered helix (A5–V17) and a more disordered helix (S20–L23), can be seen in the structure.

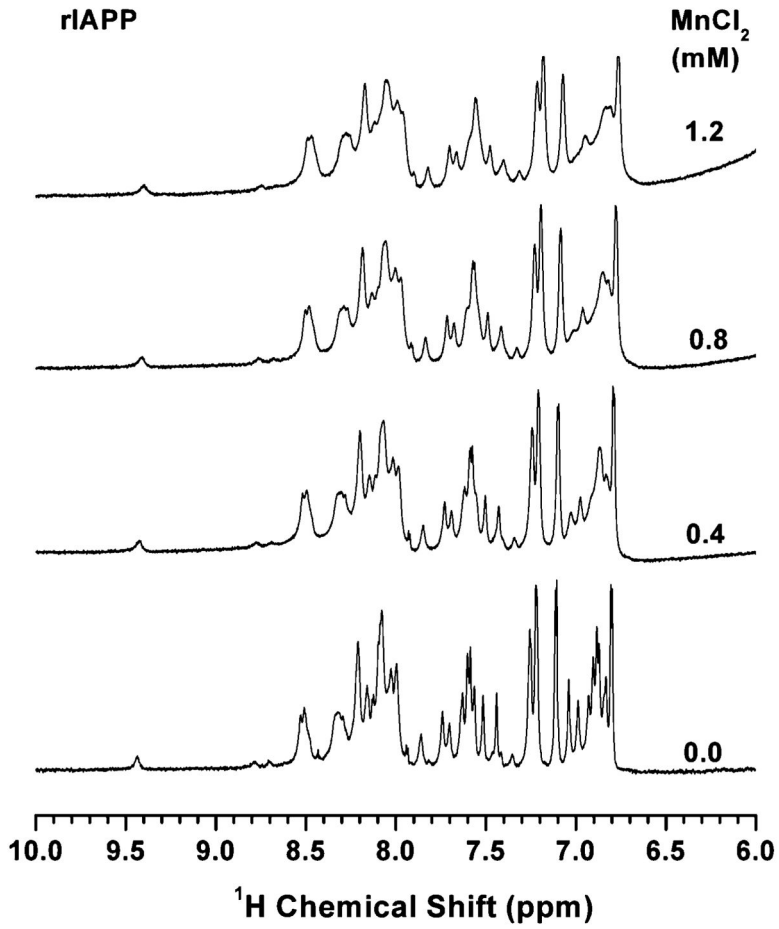

Figure 7.

Amide proton chemical shift region of ^{1}H NMR spectra of rat IAPP in DPC micelles at pH 7.3 with and without $MnCl_2$. The spectral intensities were normalized.

Figure 8.

Percentage decrease in the signal intensity of α-proton chemical shift resonances of rat IAPP embedded in DPC micelles at pH 7.3 after addition of 0.8 mM $MnCl_2$.

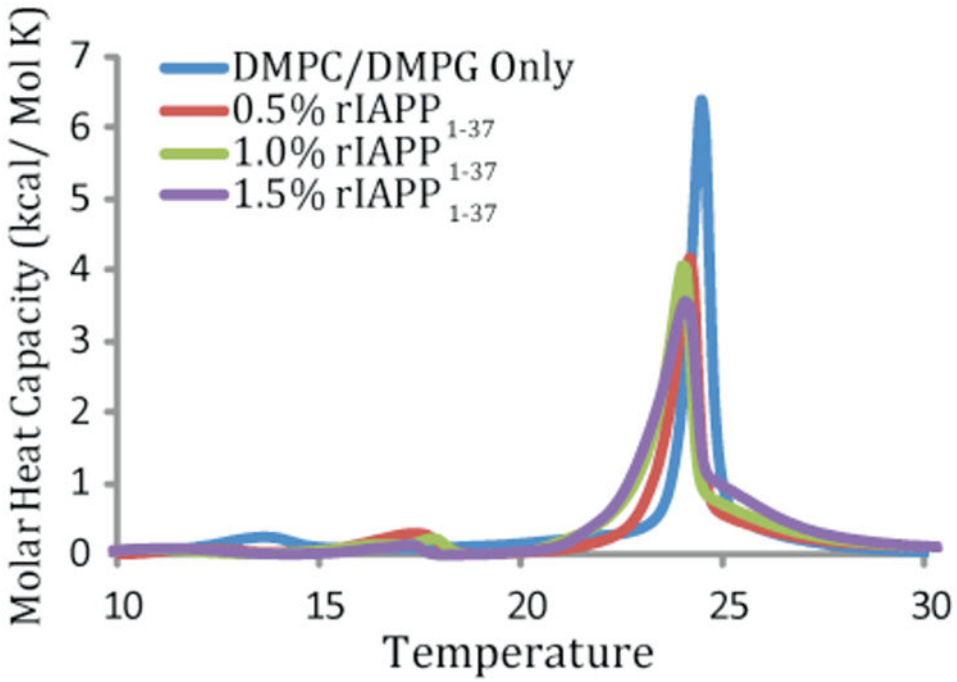

Figure 9.

Differential scanning calorimetry of the pretransition and the main gel to liquid-crystalline phase transition of DMPC/DMPG (7:3) vesicles at the indicated molar ratio of rIAPP to lipid. Peptide and lipids were codissolved in a chloroform/ethanol solution, dried, and resuspended in sodium phosphate buffer, pH 7.3 with 150 mM NaCl.

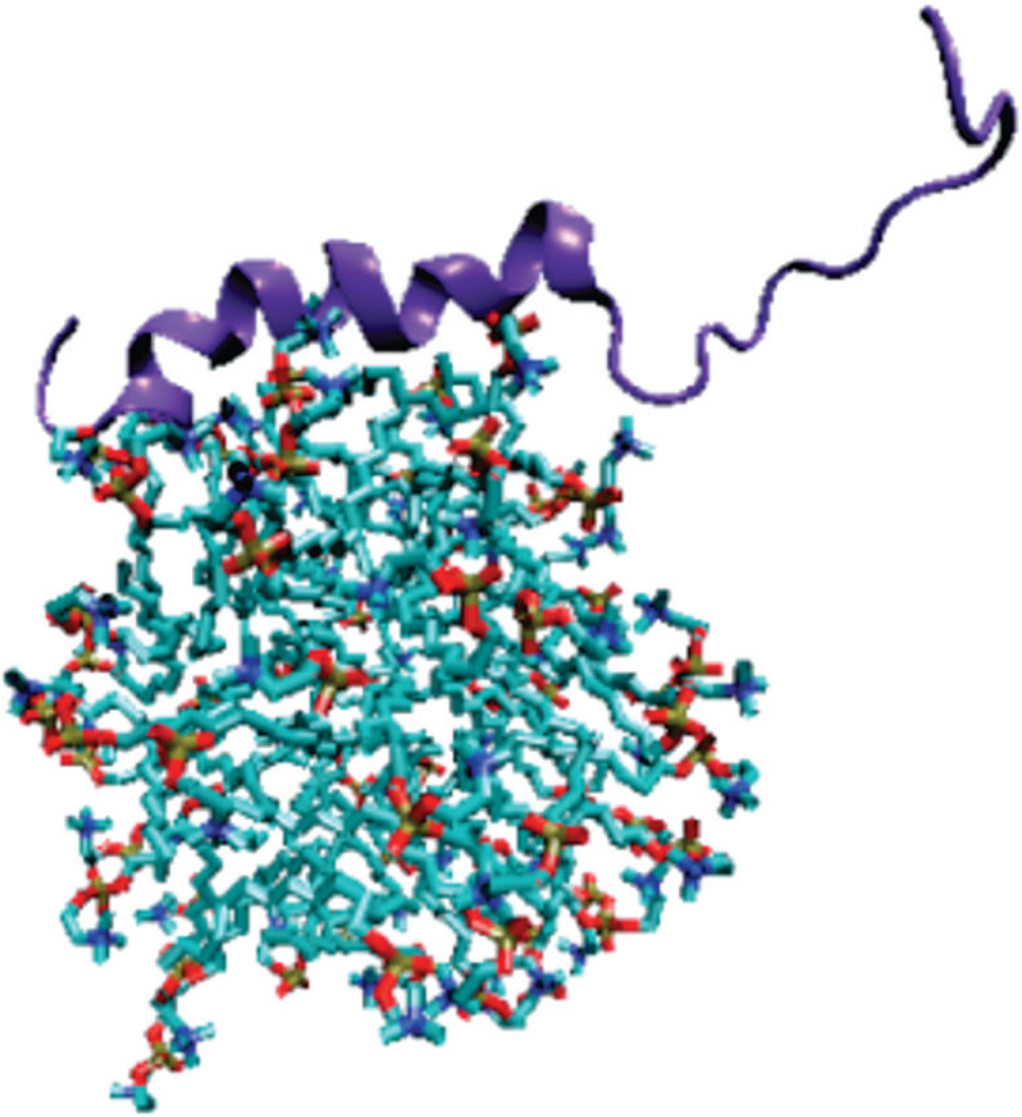

Figure 10.
Cartoon representation of rIAPP binding to the surface of the micelle. The micelle structure is from a molecular dynamics simulation of 54 DPC molecules in explicit water (ref 78).

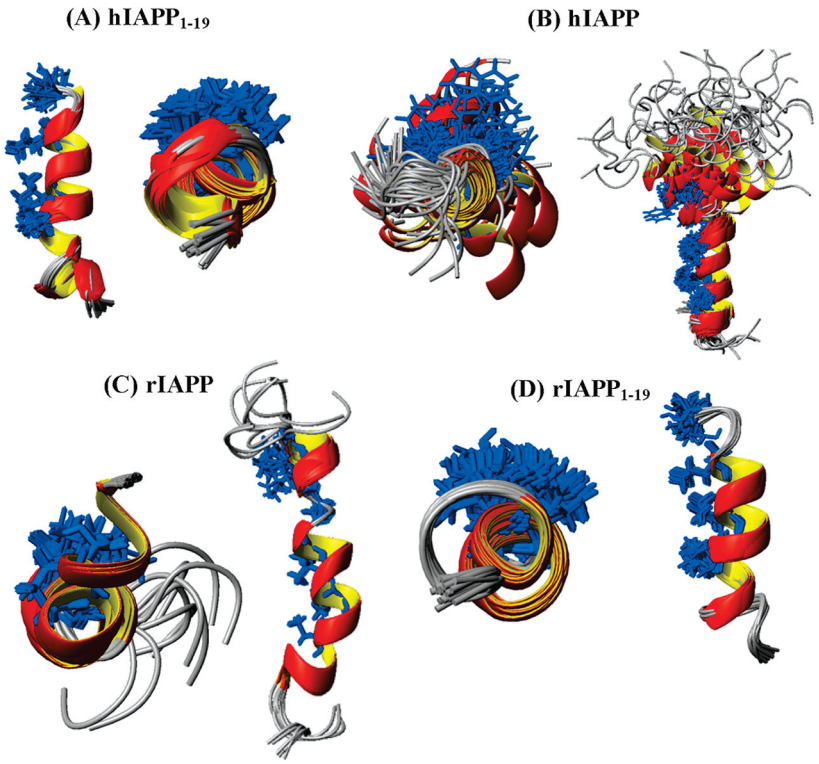

Figure 11.

Structures of $hIAPP_{1–19}$ (A), hIAPP (B), rIAPP (C), and $rIAPP_{1–19}$ (D) showing the degree of occlusion of the putative self-association site by the N-terminal loop in each structure. The hydrophobic residues that have been implicated in coiled-coil interactions stabilize the IAPP oligomer are colored in blue.

Table 1

Statistical Information for the Structural Ensemble of Rat IAPP

Distance Constraints	
total	485
intraresidual	262
inter-residual	223
sequential ($i - j = 1$)	138
medium ($i - j = 2, 3, 4$)	85
Structural Statistics	
NOE violations (Å)	0.0554 ± 0.0008
dihedral angle restraint violations (deg)	1.3053 ± 0.0609
rmsd for bond deviations (Å)	0.0051 ± 0.0010
rmsd for angle deviations (deg)	0.8158 ± 0.0180
rmsd of all backbone atoms (Å)	
Ala 5–Val 17	0.22 ± 0.07
Ala 5–Leu 23	0.52 ± 0.19
rmsd of all heavy atoms (Å)	
Ala 5–Val 17	0.72 ± 0.15
Ala 5–Leu 23	1.24 ± 0.21
Ramachandran Plot	
residues in most favored region (%)	75.9
residues in additionally allowed region (%)	20.3
residues in generously allowed region (%)	1.4
residues in disallowed region (%)	2.4